Biofilm 6 (2023) 100167

Contents lists available at ScienceDirect

Biofilm

journal homepage: www.sciencedirect.com/journal/biofilm

A microtiter peg lid with ziggurat geometry for medium-throughput antibiotic testing and *in situ* imaging of biofilms

Sarah K. Childs [1], A-Andrew D. Jones III [*]

Department of Civil & Environmental Engineering, Pratt School of Engineering, Duke University, Durham, NC, USA

A B S T R A C T

Bacteria biofilm responses to disinfectants and antibiotics are quantified and observed using multiple methods, though microscopy, particularly confocal laser scanning microscopy (CLSM) is preferred due to speed, a reduction in user error, and *in situ* analysis. CLSM can resolve biological and spatial heterogeneity of biofilms in 3D with limited throughput. The microplate peg-lid-based assay, described in ASTM E2799-22, is a medium-throughput method for testing biofilms but does not permit *in situ* imaging. Breaking off the peg, as recommended by the manufacturer, risks sample damage, and is limited to easily accessible pegs. Here we report modifications to the peg optimized for *in situ* visualization and visualization of all pegs. We report similar antibiotic challenge recovery via colony formation following the ASTM E2799-22 protocol and *in situ* imaging. We report novel quantifiable effects of antibiotics on biofilm morphologies, specifically biofilm streamers. The new design bridges the MBEC® assays design that selects for biofilm phenotypes with *in situ* imaging needs.

1. Introduction

The world is headed towards an antibacterial resistance cliff, a point where common medical procedures will risk deadly infections, expected to occur between 2030 and 2050, with failure to address this crisis estimated to cost over $1 trillion annually [1,2]. Bacteria primarily exist in biofilms, grouped together in a matrix of polymers, sugars, proteins, and extracellular DNA, which both reduce the efficacy of antibiotics and enable increased antimicrobial resistance gene transfer [3,4]. While there has been a promising shift in scientific focus from strategies targeting planktonic bacteria to bacterial biofilms [5–10], standardized *in situ* tools for imaging biofilms are still lacking [11].

Microfluidic assays to study bacterial biofilms are commonly used but are limited in throughput and have been difficult to standardize [11–13]. Microfluidic assays have allowed for facile visualization with fluorescent microscopes enabling *in situ* understandings of biofilm development and dispersal [11–13]. Microfluidic assays are easy to produce and customize. ASTM International standardized methods for biofilm research and other proposed biofilm research protocols are notably repeatable, fast, and reliant on accessible supplies like coupons and conical tubes or a combination [14]. Moreover, there are four ASTM International-approved standardized devices for studying biofilms: the CDC biofilm reactor [15,16], a drip flow reactor [17], a rotating disk reactor [16], and the MBEC Assay® or similar peg lid microtiter plate assays all with limited *in situ* microscopy access [15,18,19]. The MBEC Assay® is a 96-well plate lid with pegs that sit in the wells [20].

Microtiter biofilm assays can be used to quantify biofilm growth to assess antibiotic or disinfectant susceptibility with many methods including crystal violet staining, microscopy, or live cell counts [21]. For example, *Pseudomonas aeruginosa* biofilm metabolic activity in the presence of multiple antibiotic concentrations and combinations was rapidly screened for in a high-throughput 384-well plate device using automated, single focal plane microscopy and image analysis [22]. Protocols have recently been proposed to use confocal microscopy and plate readers to analyze antibiotic susceptibility using medium throughput 96-well plate in ~60 h and 4 -5 days respectively [23,24]. Finally, the Fluxion Bioflux device tries to merge the visualization capabilities of microfluidics with the speed of medium throughput devices by introducing a microfluidic system between wells of a 24 or 96 well plate platform, to varying degrees of success [25]. These studies, protocols, and devices highlight the application of *in situ* microscopy in biofilm studies and its potential in microtiter assays.

Two limitations of the microtiter biofilm assay addressed by the MBEC Assay® include high variation between wells [26] and settled planktonic cells erroneously counted as biofilm [11,26,27]. The MBEC Assay® produces similar biofilms across the 96 pegs [20,28] and restricts biofilm bacteria to those cells actively attaching to or growing on the pegs. The MBEC Assay® is used to establish biofilms and challenge those biofilms with an antimicrobial or disinfectant [27] enabling measurement of a minimum biofilm eradication concentration similar to

* Corresponding author.
E-mail address: andrew.jones3@duke.edu (A.-A.D. Jones).
[1] Present address: Department of Biology, Eastern Carolina University, Greenville, NC, USA.

https://doi.org/10.1016/j.bioflm.2023.100167
Received 26 July 2023; Received in revised form 9 November 2023; Accepted 9 November 2023
Available online 17 November 2023

a planktonic culture's minimum inhibitory concentration.

However, the peg lid microtiter plate assay limits the ability to image the biofilm *in situ*. The primary manufacturer of the peg lids and other protocols suggest using pliers to break off pegs for imaging and other tests [27,29,30] which is difficult to do without disrupting or contaminating the pegs demonstrated in SI Figure S1 [31]. The lack of *in situ* optical access also significantly increases the time and materials necessary to analyze the biofilms [23]. Furthermore, successful images of biofilms formed on the MBEC Assay® are generally flat and lack complex formations seen in other *in situ* assays such as microfluidic cells [30,32,33]. To enable *in situ* imaging of complex biofilm features while maintaining the through-put features of the original assay, we evaluated multiple geometries for their capacity to be imaged under confocal microscopy (see SI Figures S2, S5 – S11). We performed an early-stage evaluation on one of the design geometries, a ziggurat inspired cone, to determine if it could replicate the existing standardized protocol for the MBEC® assay. This paper presents a geometry optimized for biofilm imaging under confocal microscopy that maintains the throughput features of the original assay while showing results that previously were only accessible in microfluidic devices.

2. Results

We tested six redesigns (see SI Figure S2) of the geometry of a plate cap for a 24 well plate to image biofilms *in situ* using confocal scanning fluorescence microscopy (see SI Figures S5 - S11). We tested the final geometry, shown in Fig. 1 (A-C), against a modified version of original protocol Fig. 1 (D). We performed *in situ* confocal scanning fluorescence microscopy and gained additional quantitative information on the impact of antibiotics on biofilm streamers.

2.1. Standardized methods

We evaluated the ziggurat peg-lid's applicability to the relevant ATSM standard, E2799-22, modified workflow Fig. 1 (D) [34]. The modified peg plate lid could be handled in the same fashion as the commercially available peg lid. The pegs were less rigidly attached to the lid than the commercially available peg lid and could be broken off easily for a biofilm growth check, although due to the ring of biofilm at the air-medium interface typical of wild-type PA14 [35], this could also be verified visually. Due to the design, it was also possible to image *in situ*. After imaging, OD 600 and CFU counts were performed to verify no loss of function between the peg plate optimized for imaging and the commercially available peg lid, Fig. 2 (A-C). Using tetracycline as the antibiotic challenge, observed 0 and 3-fold reduction in CFU on a per area basis at 10 and 100 μg/mL. Relative to the area of the MBEC® Assay, 46.63 mm^2 the area of this peg presents a 6.5 fold increase to 302.1 mm^2. Using OD600, we observed a 0.02 and 0.03 mean reduction

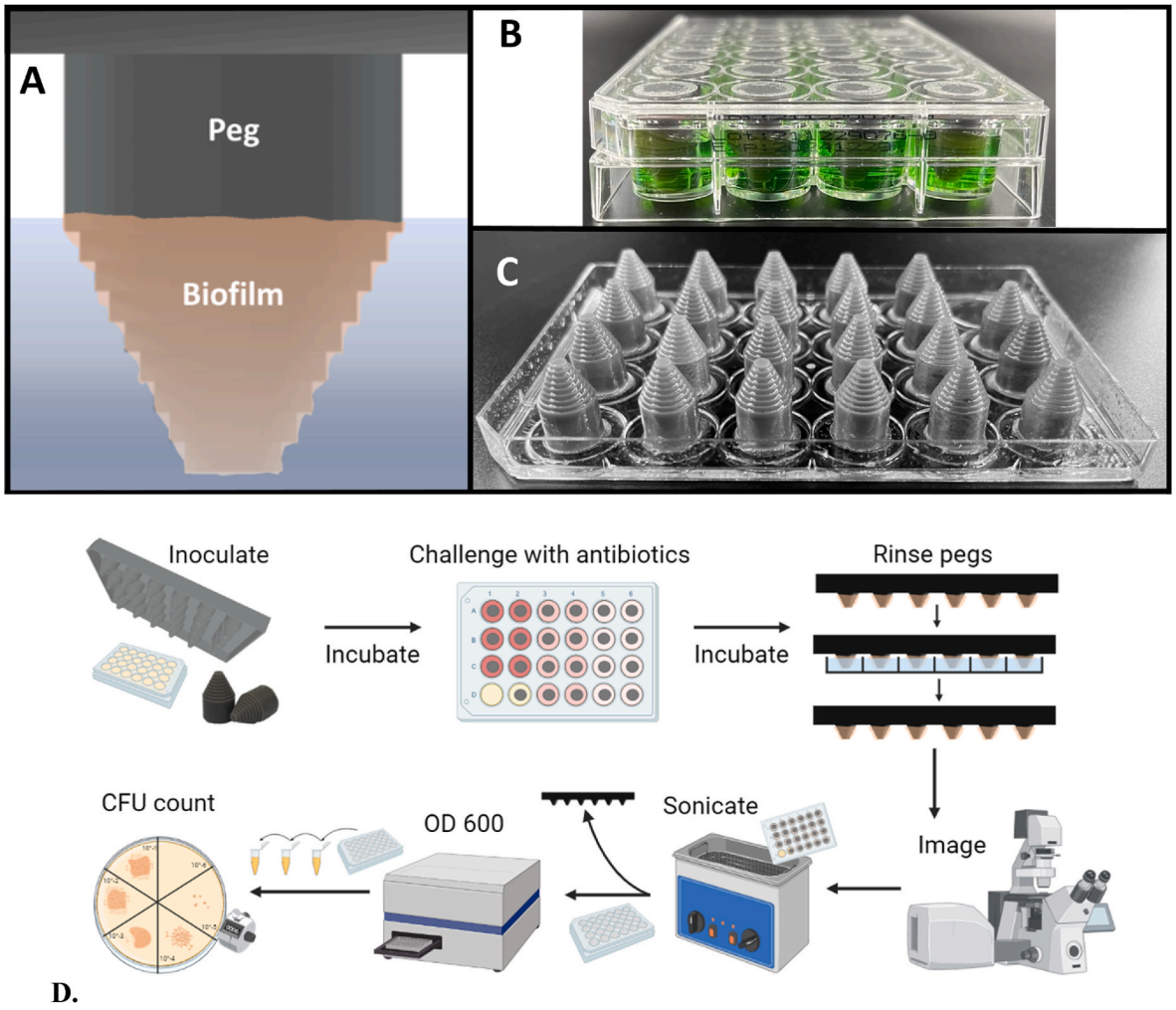

Fig. 1. The final design of the modified peg plate. **(A)** Biofilm forms on the peg structure. **(B)** The peg lid is immersed in 1.5 mL media (represented in green). **(C)** 23 individual pegs are attached to the lid of a 24-well plate. One well does not contain a peg as a broth sterility check. **(D)** Workflow diagram that shows the antibiotic challenge experimental process using the peg plate design. (For interpretation of the references to colour in this figure legend, the reader is referred to the Web version of this article.)

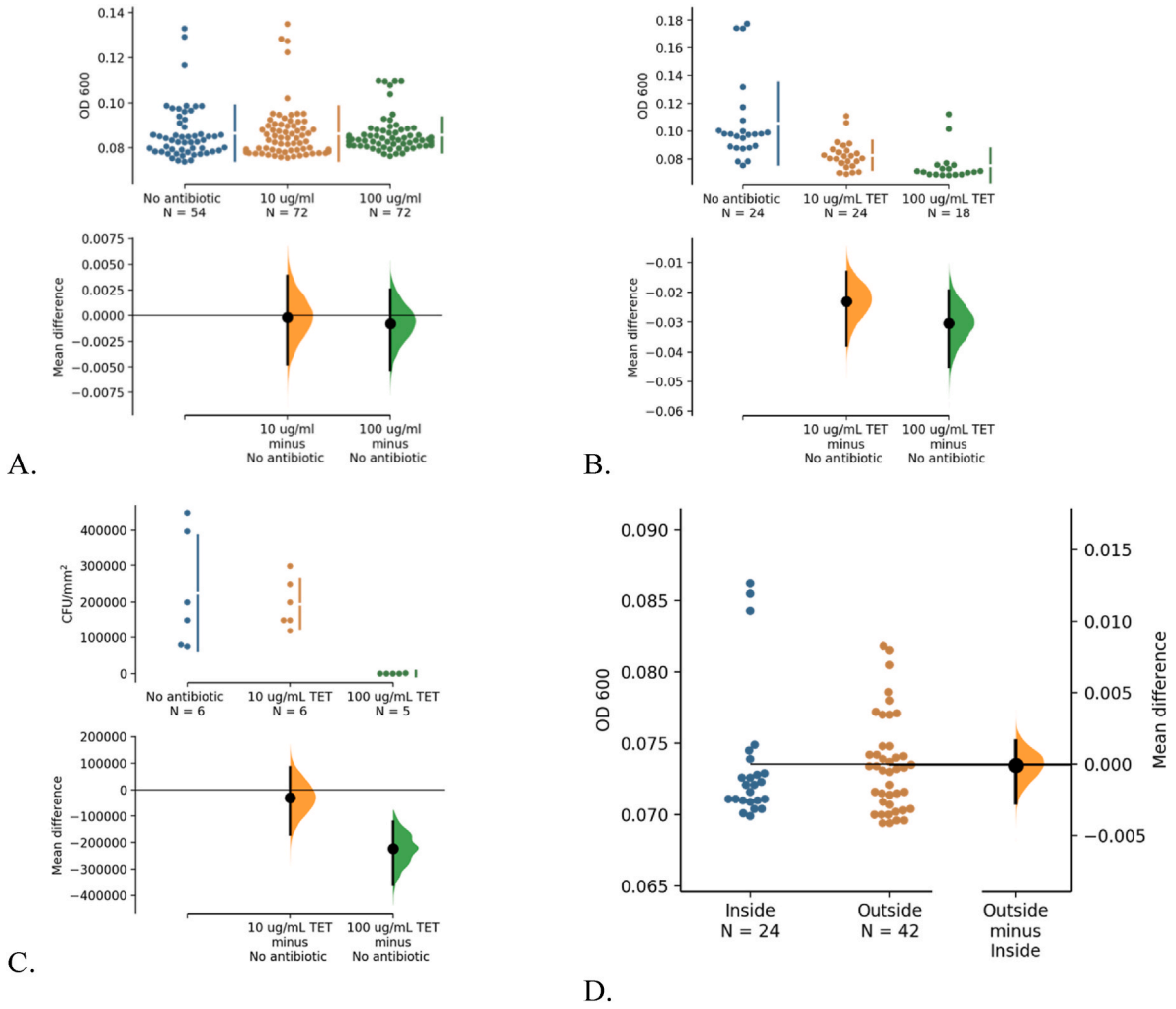

Fig. 2. The raw data and mean difference versus no antibiotics are shown for 100 μg/mL tetracycline, 10 μg/mL tetracycline on an OD 600 basis on the (A) MBEC® Assay, (B) the modified plate, and (C) on a CFU/mm^2 for PA14. (3 technical replicates, 2 biological replicates for CFU counts and 3 technical replicates, 6 (100 μg/mL tetracycline) and 8(10 μg/mL tetracycline and no antibiotic) biological replicates for OD600). **(D)** Equivalent biofilm test using OD 600 readings of biofilm recovered in PBS by sonication from the ziggurat peg design. PA14 was grown on pegs in TSB for 24 h before recovery. Wells were categorized as "inside" or "outside" according to the layout in Fig. 4 (B). The mean differences is plotted using bootstrap sampling distributions and 95 % confidence interval is indicated by the ends of the vertical error bars using EstimationStats [38].

at 10 and 100 μg/mL respectively which is similar to what we saw with the MBEC® Assay. These results agree with the literature on tetracycline against *P. aeruginosa* PAO1 biofilms with a similar intermediate concentration (0 - 8 μg/mL tetracycline) and strain MTCC 2488 with lower concentrations (0 and 2 μg/mL tetracycline) [36,37]. We performed an equivalent growth test in TSB with the peg lids showing a negligible mean difference between the inner and outer pegs, in Fig. 2 (D).

2.2. Microscopy results

The intent of this redesign is to optimize for *in situ* confocal imaging. We applied two imaging techniques to evaluate this. The surface of the bottom step of the ziggurat design was captured using a tile and z-stack approach. The biomass formed on the edges of the peg and, in the "no antibiotic" samples, could be thick enough to scatter the fluorescent light emission [39]. This is known to leave imaging artifacts resembling "holes" in the images observed in Fig. 3 (A) "No antibiotic" (see also, SI Figure S12) [39]. The space between steps formed biofilm streamers, as can be seen in Fig. 3 (B). The biofilms formed without antibiotics were robust and thick while the streamers formed under low levels of tetracycline were less frequent and thin. For example, in Fig. 3 (B), the streamer produced by PA14 in the presence of 10 μg/mL has an approximate midpoint diameter of 40.05 ± 11.98 μm which was 12.96 % of the no antibiotic streamer at 309.09 ± 10.43 μm. Similar to what was shown by the CFU count and OD 600 measurements, biomass (μm^3/μm^2) increased as antibiotic concentration decreased, although there was a low sample size.

3. Discussion

This early-stage evaluation of a redesign of MBEC® assay was motivated by the need to add *in situ* imaging capability to microtiter assays of bacterial biofilms. While we considered six geometries, all but one was rejected due to various troubleshooting issues (see SI Figures S2, S3, S5 – S11). The final design was tested against the original protocol in addition to *in situ* microscopy. The remaining design, the ziggurat, was validated against an antibiotic challenge of *P. aeruginosa* PA14. This alternative peg design was able to complete a modified ASTM 2799 protocol with the addition of CLSM. We not only found that we could repeat the original protocol, but also that we could observe known complex biofilm morphologies and quantify their response to antibiotic challenges.

The ziggurat geometry provides more dynamic views of structures than a flat surface. We observed biofilm streamers in Fig. 3 (B) for no

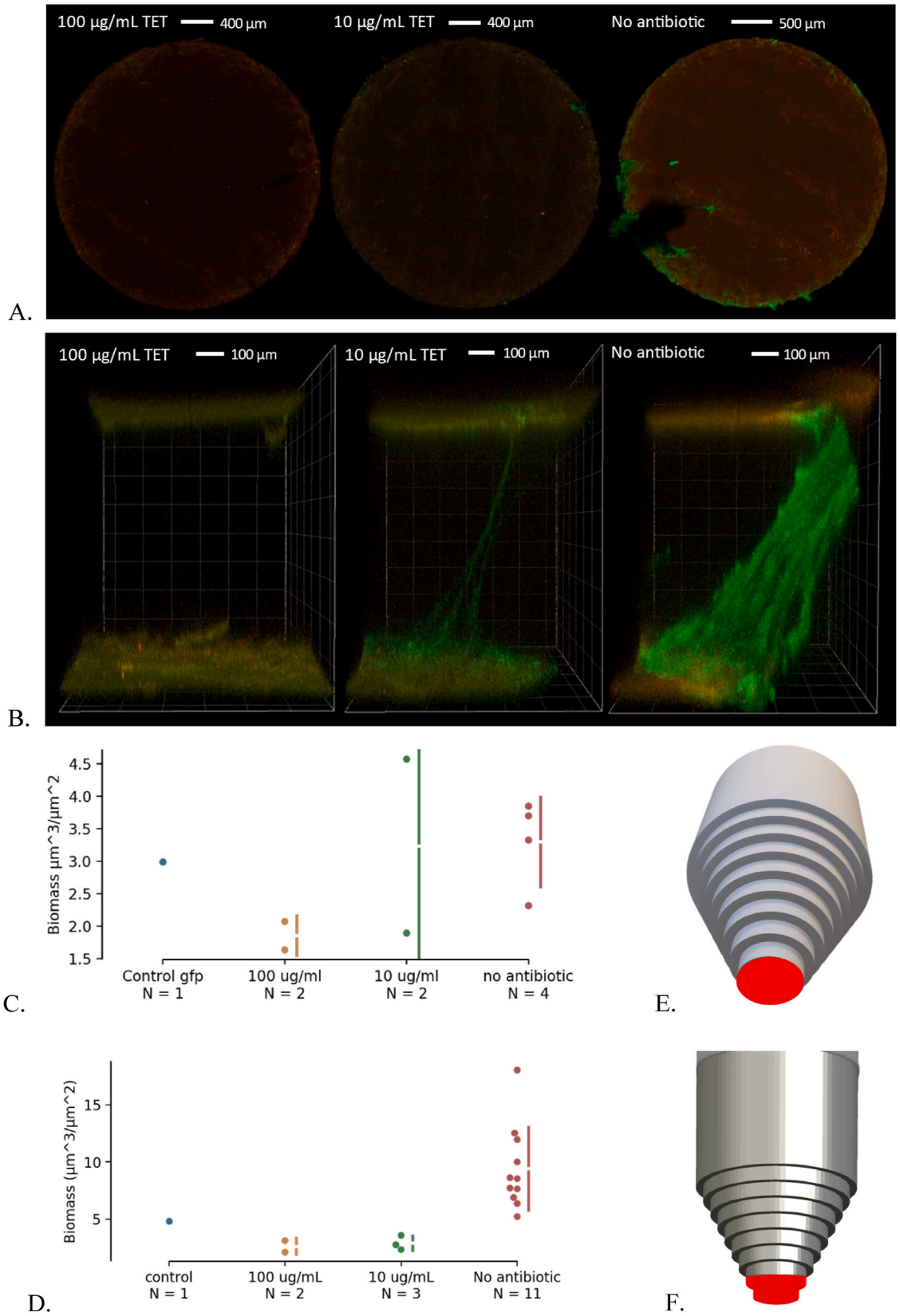

Fig. 3. **(A)** Selected 3D tiles of the surface of the bottom step of the peg with an area of 8.042 mm^2, green is the bacteria, red is the autofluorescent peg. **(B)** Selected Z-stacks of the space between the bottom step and the second step. Streamers often formed in this area. **(C)** The surface biomass on the bottom step analyzed using COMSTAT 2.1 was plotted using EstimationStats [38]. **(D)** The biomass on the second step of the ziggurat step analyzed using COMSTAT 2.1 was plotted using EstimationStats [38]. **(E)** Shows the area imaged in (A) on the peg's CAD model. **(F)** Shows the area imaged in (B) on the peg's CAD model. (For interpretation of the references to colour in this figure legend, the reader is referred to the Web version of this article.)

A.

	1	2	3	4	5	6
A	100	100	10	10	0	0
B	100	100	10	10	0	0
C	100	100	10	10	0	0
D	BC	PC	10	10	0	0

B.

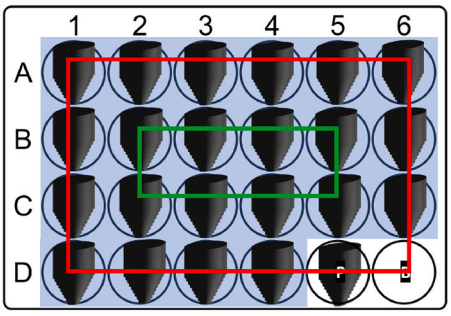

Fig. 4. (A) An example of a challenge plate layout. The layout contains 3 concentrations of antibiotic: 100 μg/mL tetracycline, 10 μg/mL tetracycline, and no antibiotic. Two uninoculated controls are included the BC (broth control, no peg) and PC (peg control) checking for media and device sterility respectively. **(B) Layout of equivalent biofilm test plate.** The blue highlighting indicates wells with TSB and PA14. P indicates the peg control well and B indicates the broth control well. During analysis, pegs on the red line were considered the outside pegs and pegs on the green line were considered inside pegs. (For interpretation of the references to colour in this figure legend, the reader is referred to the Web version of this article.)

antibiotic and 10 μg/mL of antibiotic. Biofilm streamers were first reported *in situ* by Stoodley and Lewandowski under turbulent flow conditions [40]. Biofilm streamers are biofilms that are high-aspect ratio aggerates attached to at least one surface extending into a flow field. They are best measured using *in situ* microscopy methods and can also be quantified using pressure transducers as they produce oscillatory changes in pressure [40]. Biofilm streamers have since been replicated under laminar flow conditions [41,42], implicated in pressure loss in mechanical systems [43] clogging of porous media, blood vessels, and heart valves [44,45]. Effects of antibiotics on dispersion and clogging have been measured, showing limited effect, however effects on the structure and thickness of the streamer itself were not reported [44]. Model systems for studying streamers have been micro or millifluidic devices that could be mounted onto microscopes as most studies consider streamers as functions of the fluid interaction with obstructing geometries [43]. Specifically, biofilm streamers have been noted to form on secondary vortices where biofilms form on free surfaces [41,42,44]. Here we observed a quantifiable reduction in thickness under antibiotic challenge. While the 24-well plate is in laminar flow at 100 rpm [46], it is reasonable, but remains to be shown if there are secondary vortices forming at the right-angle of the two steps where the streamer formed. Since bulk material strength is proportional to material thickness, the ability to observe this weakening is useful information gained by *in situ* microscopy. These streamers have not been described in work utilizing the MBEC® system or microtiter assays, though it may be reasonable to assume that streamers could form between the apex of the peg and well if imaged *in situ* [30,33]. As has been the case in other *in situ* imaging studies of microtiter plates, imaging and biomass computation takes excessive time, which may limit usefulness of this and other implementations of imaging microtiter assays [23,24]. Subsequently, we did not repeat the biomass measurements enough to report statistical significance.

Selection of peg materials impacted sterilization and imaging quality. For a reusable device, the material must be resistant to UV and chemicals used in cleaning such as sodium hypochlorite and isopropyl alcohol which eliminates some resins used in stereolithography. For high image quality, the material must also be minimally autofluorescence to prevent complications during biofilm quantification. The material selection is further described in the supplemental information. With the advent of additive manufacturing, other 3D printers could leverage other plastics, glass, metals, and/or 3D bioprinters could produce biological materials to perform similar studies.

The ziggurat peg design compared to microtiter and the MBEC® assay. Relative to the MBEC® assay, microscopy can be performed *in situ* allowing image collection from multiple pegs without reducing the number of samples for the OD 600 and CFU count. Furthermore, the imaged pegs are not limited to the outer edges of the plate as in the MBEC® assay [27,29]. Additionally, relative to the MBEC® assay, the pegs did not need to be extensively handled, which reduced the risk of contamination or disruption of the biofilm. The ziggurat peg design compared to the microplate assay has a longer working distance. However, the outer wells of microtiter plates are known to suffer from "edge effects" as a result of uneven evaporation and temperature distributions, so imaging and other results from the interior is preferred [47]. Furthermore, the ziggurat peg design allows for biofilm morphologies to be imaged including streamers.

The MBEC® assay was an improvement of the microtiter plate assay recognizing that studies of bacterial biofilm growth and disruption required a high-throughput assay collecting more representative data. However, the MBEC® assay reduced the capability for *in situ* imaging that has also become a feature of microtiter assays and biofilm studies. Here we report a ziggurat peg design that maintains existing MBEC® protocols while adding *in situ* CLSM imaging. The ziggurat geometry also allowed for the formation of biofilm streamers that opens possibilities for medium-throughput screening of biofilm fluid-structure antibiotic interactions. While we have only examined the device at a single time point to show the fidelity with existing protocols, the ziggurat peg design enables *in situ* observations of dynamic biofilm responses to antibiotics. Furthermore, it could enable examination biofilm streamer response to the addition of antimicrobials or changes in nutrients. This design merges the successful features of the microtiter plate assay and the MBEC® assay to build an easy-to-implement and flexible assay for examining biofilms.

4. Materials and methods

4.1. Peg-lid production

Six distinct modified pegs geometries (SI Figure S2) were designed using Autodesk Fusion 360 and 3D printed with Durable Resin (Formlabs, USA), for the initial designs, or Tough 1500 Resin (Formlabs, USA), for the final design. 3D printing was performed using a Formlabs Form 2 low-force stereolithography 3D printer (see discussion in SI on resin choice). Prior to use, pegs were soaked in 1–2% solution of Citranox detergent (VWR International, USA), rinsed with deionized water, and air dried. Pegs were fixed to a sterile 24-well plate lid using a small drop of clear nitrocellulose nail varnish and sterilized with a UV lamp. After use, pegs were soaked in a 0.5–0.7 % solution of sodium hypochlorite, removed from the plate lid, vortexed in acetone to remove remaining nail varnish, and cleaned for reuse.

4.2. Bacterial strain and growth condition

Experiments were conducted using *Pseudomonas aeruginosa* PA14

which constitutively expressed GFP [48]. Cultures were grown overnight in tryptic soy broth (VWR International, USA) at 37 °C and 150 rpm. 10 μL of the overnight culture was used to inoculate 50 mL of fresh TSB. The growth plate (24 well, VWR International, USA) was prepared by dispensing 8 mL of broth per well, adding the peg lid, and incubating for 24 h at 37 °C and 100 rpm. The antibiotic challenge plate was prepared (layout in Fig. 4 (A)) and the peg lid was transferred from the growth plate and incubated for 24 h at 37 °C and 100 rpm [49,50].

Transfers between media and rinse plates were accomplished by lifting the peg lid, allowing excess liquid to drip off, and gently placing the lid in the new plate. Before imaging, the peg lid was rinsed in sterile deionized water and placed in phosphate-buffered saline (PBS). One of the challenges with microtiter assays is uniform growth across wells, potentially due to uneven heat transfer and evaporation rates. We performed an equivalent growth test in TSB with the peg lids, layout in Fig. 4 (B). We did not test the efficacy of removal from the surface by sonication, however the resultant OD600 readings for *P. aeruginosa* between this and the MBEC® assay were similar.

ASTM standard 2799-22 was followed with five deviations to fit the experiment and modified design. The first deviation was that serial dilutions of the inoculum were not performed. The second deviation was that a biofilm growth check was not performed. The third deviation was that the challenge plate layout was altered to fit a 24-well plate. The fourth deviation was that the biofilm growth time was increased from 16-18 h to 24 h prior to the antibiotic challenge. The final deviation was the peg lid was transferred into a recovery plate for neutralization by dilution as opposed to neutralizer since antibiotics were being tested [27].

4.3. Standardized methods

After imaging, the peg lid suspended in PBS was sonicated on high for 30 ± 5 min using a Branson ultrasonic bath (Branson Ultrasonics, USA). The peg lid was removed and replaced with a standard lid before taking an OD 600 reading of PBS recovery plate using a SpectraMax i3x plate reader (Molecular Devices, USA). A serial dilution was then performed on a selected row and spot-plated onto TSA for enumeration of CFU attached to the peg. A simplified workflow diagram of the described procedure is shown in Fig. 1 (D).

4.4. Microscopy methods

Pegs were imaged in PBS with an inverted Zeiss LSM 900 (Zeiss, Germany) using a 488 nm laser for excitation and detection wavelengths of 410-546 nm (green) for GFP and 590-700 nm (red) for identifying autofluorescence. Imaging was conducted using a 10X objective to compensate for the increased working distance. Images were taken by stitching square tiles (585 x 585 μm, 469 x 469 pixels) of the peg surface with or without Z-stacks (See SI Figure S4). The steps on the ziggurat, the final design selected, were also imaged using Z-stacks. Biomass quantification of antibiotic plate images was performed using Comstat2 v2.1 as an ImageJ plugin [51–54].

4.5. Statistical methods

Estimation statistics were used to quantify the magnitude of the effect of each concentration of antibiotic challenge relative to the no antibiotic control. CFU counts were all performed using 2 wells per condition and 3 replicate plates per well. OD 600 readings were performed using all wells per condition with 3 replicates per well. Biomass quantification was performed using available confocal images. All data is presented and analyzed using a Cummings estimation plot produced using EstimationStats [38]. This displays both the raw data (upper axis) and the mean difference for 2 comparisons against the shared control (lower axis) plotted as bootstrap sampling distributions with the ends of the vertical error bars indicating a 95 % confidence interval. When the sample size was too low (specifically the analyzed images, see Fig. 3), mean difference was not included.

Funding

Research reported in this publication was supported by the National Institute of General Medical Sciences of the National Institutes of Health under Award Number NIH R35 GM142898 (SKC, AJ). The content is solely the responsibility of the authors and does not necessarily represent the official views of the National Institutes of Health.

Data and materials availability

All data are available in the main text or the supplementary materials. Raw data files are available upon request.

CRediT authorship contribution statement

Sarah K. Childs: Conceptualization, Methodology, Validation, Formal analysis, Investigation, Data curation, Writing – original draft, Writing – review & editing, Visualization. **A-Andrew D. Jones:** Conceptualization, Methodology, Writing – original draft, Writing – review & editing, Supervision, Project administration, Funding acquisition.

Declaration of competing interest

The authors declare the following financial interests/personal relationships which may be considered as potential competing interests: Akhenaton-Andrew Dhafir Jones, III has patent #63/438,666 pending to Duke University. Sarah Kate Childs has patent #63/438,666 pending to Duke University.

Data availability

Data will be made available on request.

Acknowledgments

Lingchong You provided the constitutively expressing *P. aeruginosa* PA14 *GFP* strain. 3D printing was provided by Duke University's Innovation Co-Lab.

Appendix A. Supplementary data

Supplementary data to this article can be found online at https://doi.org/10.1016/j.bioflm.2023.100167.

References

[1] Ventola CL. The antibiotic resistance crisis: part 1: causes and threats. P T 2015;40(4):277–83.
[2] Dadgostar P. Antimicrobial resistance: implications and costs. Infect Drug Resist 2019;12:3903–10.
[3] Wu F, et al. Modulation of microbial community dynamics by spatial partitioning. Nat Chem Biol 2022;18(4):394–402.
[4] Yao Y, et al. Intra- and interpopulation transposition of mobile genetic elements driven by antibiotic selection. Nat Ecol Evol 2022;6(5):555–64.
[5] Sutherland I. The biofilm matrix – an immobilized but dynamic microbial environment. Trends Microbiol 2001;9(5):222–7.
[6] Costerton JW, Stewart PS. Battling biofilms. Sci Am 2001;285(1):74–81.
[7] Stoodley P, et al. Evolving perspectives of biofilm structure. Biofouling 1999;14(1):75–90.
[8] Lewis K. Riddle of biofilm resistance. Antimicrob Agents Chemother 2001;45(4):999–1007.
[9] Dunne WM. Bacterial adhesion: seen any good biofilms lately? Clinical Microbiology Reviews 2002;15(2):155–66.
[10] Stoodley P, et al. Biofilms as complex differentiated communities. Annu Rev Microbiol 2002;56:187–209.
[11] Azeredo J, et al. Critical review on biofilm methods. Crit Rev Microbiol 2017;43(3):313–51.

[12] Pousti M, et al. Microfluidic bioanalytical flow cells for biofilm studies: a review. Analyst 2018;144(1):68–86.
[13] Perez-Rodriguez S, Garcia-Aznar JM, Gonzalo-Asensio J. Microfluidic devices for studying bacterial taxis, drug testing and biofilm formation. Microb Biotechnol; 2021.
[14] Allkja J, et al. Interlaboratory study for the evaluation of three microtiter plate-based biofilm quantification methods. Sci Rep 2021;11(1):13779.
[15] Allkja J, et al. Minimum information guideline for spectrophotometric and fluorometric methods to assess biofilm formation in microplates. Elsevier B.V; 2019. p. 100010. 100010.
[16] E2562-17, A. Standard test method for quantification of Pseudomonas aeruginosa biofilm grown with high shear and continuous flow using CDC biofilm reactor. ASTM Int. West Conshohocken PA; 2017.
[17] E2647-08, A. Standard test method for quantification of a Pseudomonas aeruginosa biofilm grown using a drip flow biofilm reactor with low shear and continuous flow. West Conshohocken PA: ASTM Int.; 2008.
[18] Leid JG, et al. The exopolysaccharide alginate protects Pseudomonas aeruginosa biofilm bacteria from IFN- -mediated macrophage killing. J Immunol 2005;175 (11):7512–8.
[19] E2799-17, A. Standard test method for testing disinfectant efficacy against Pseudomonas aeruginosa biofilm using the MBEC assay. ASTM Int. West Conshohocken PA; 2017.
[20] Ceri H, M.E O, Stremick C, Read RR, Morck D, Buret A. The calgary biofilm device: new technology for rapid determination of antibiotic susceptibilities of bacterial biofilms. J Clin Microbiol 1999;37(6):1771–6.
[21] Latka A, Drulis-Kawa Z. Advantages and limitations of microtiter biofilm assays in the model of antibiofilm activity of Klebsiella phage KP34 and its depolymerase. Sci Rep 2020;10.
[22] Navarro G, et al. Image-based 384-well high-throughput screening method for the discovery of skyllamycins A to C as biofilm inhibitors and inducers of biofilm detachment in Pseudomonas aeruginosa. Antimicrob Agents Chemother 2014;58 (2):1092–9.
[23] Haney EF, Trimble MJ, Hancock REW. Microtiter plate assays to assess antibiofilm activity against bacteria. Nat Protoc 2021;16(5):2615–32.
[24] Musken M, et al. A 96-well-plate-based optical method for the quantitative and qualitative evaluation of Pseudomonas aeruginosa biofilm formation and its application to susceptibility testing. Nat Protoc 2010;5(8):1460–9.
[25] Romero M, et al. Mushroom-shaped structures formed in Acinetobacter baumannii biofilms grown in a roller bioreactor are associated with quorum sensing-dependent Csu-pilus assembly. Environ Microbiol 2022;24(9):4329–39.
[26] Kasper Nørskov Kragh MA, Kvich Lasse, Bjarnsholt Thomas. Into the well—a close look at the complex structures of a microtiter biofilm and the crystal violet assay, 1. Biofilm; 2019.
[27] Harrison JJ, et al. Microtiter susceptibility testing of microbes growing on peg lids: a miniaturized biofilm model for high-throughput screening. Nat Protoc 2010;5: 1236–54.
[28] Harrison JJ, et al. Copper and quaternary ammonium cations exert synergistic bactericidal and antibiofilm activity against Pseudomonas aeruginosa. Antimicrob Agents Chemother 2008;52(8):2870–81.
[29] MBEC Assay. For high-throughput antimicrobial susceptibility testing of biofilms procedural manual. 2.1 ed. Edmonton, Alberta: Innovotech Inc; 2019.
[30] Harrison JJ, et al. The use of microscopy and three-dimensional visualization to evaluate the structure of microbial biofilms cultivated in the Calgary Biofilm Device. Biol Proced Online 2006;8(1):194–215.
[31] Ali L, Khambaty F, Diachenko G. Investigating the suitability of the Calgary BioWlm Device for assessing the antimicrobial efficacy of new agents. Bioresour Technol 2006;97(15):1887–93.
[32] Harrison JJ, et al. Metal ions may suppress or enhance cellular differentiation in Candida albicans and Candida tropicalis biofilms. Applied and Enviromental Microbiology 2007;73(15):4940–9.
[33] Parahitiyawa NB, et al. Interspecies variation in Candida biofilm formation studied using the Calgary biofilm device. Journal of Pathology, Microbiology, and Immunology 2006;114(4):298–306.
[34] International A. Standard test method for testing disinfectant efficacy against Pseudomonas aeruginosa biofilm using the MBEC assay. 2022.
[35] O'Toole GA, Kolter R. Flagellar and twitching motility are necessary for Pseudomonas aeruginosa biofilm development. Mol Microbiol 1998;30(2): 295–304.
[36] Khan F, et al. Streptomycin mediated biofilm inhibition and suppression of virulence properties in Pseudomonas aeruginosa PAO1. Appl Microbiol Biotechnol 2020;104(2):799–816.
[37] Dey P, et al. Naringin sensitizes the antibiofilm effect of ciprofloxacin and tetracycline against Pseudomonas aeruginosa biofilm. International Journal of Medical Microbiology 2020;310(3).
[38] Ho J, et al. Moving beyond P values: data analysis with estimation graphics. Nat Methods 2019;16(7):565–6.
[39] De Souza N. Optical imaging in thick samples. Nat Methods 2009;6(1):35. 35.
[40] Stoodley P, Lewandowski Z. Flow induced vibrations, drag force, and pressure drop in conduits covered with biofilm. Water Sci Technol 1995;32(8):19–26.
[41] Rusconi R, et al. Secondary flow as a mechanism for the formation of biofilm streamers. Biophys J 2011;100(6):1392–9.
[42] Rusconi R, et al. Laminar flow around corners triggers the formation of biofilm streamers. J R Soc Interface 2010;7(50):1293–9.
[43] Stoodley P, et al. Oscillation characteristics of biofilm streamers in turbulent flowing water as related to drag and pressure drop. Biotechnol Bioeng 1998;57(5): 536–44.
[44] Drescher K, et al. Biofilm streamers cause catastrophic disruption of flow with consequences for environmental and medical systems. Proc Natl Acad Sci U S A 2013;110(11):4345–50.
[45] Valiei A, et al. A web of streamers: biofilm formation in a porous microfluidic device. Lab Chip 2012;12(24).
[46] Durauer A, et al. Mixing at the microscale: power input in shaken microtiter plates. Biotechnol J 2016;11(12):1539–49.
[47] Mansoury M, et al. The edge effect: a global problem. The trouble with culturing cells in 96-well plates. Biochemistry and Biophysics Reports 2021;26.
[48] Luo N, et al. Collective colony growth is optimized by branching pattern formation in Pseudomonas aeruginosa. Mol Syst Biol 2021;17(4).
[49] Fauzia Kartika Afrida, M M, Syam Ari Fahrial, Waskito Langgeng Agung, Doohan Dalla, Rezkitha Yudith Annisa Ayu, Matsumoto Takashi, Tuan Vo Phuoc, Akada Junko, Yonezawa Hideo, Kamiya Shigeru, Yamaoka Yoshio. Biofilm formation and antibiotic resistance phenotype of Helicobacter pylori clinical isolates. Toxins 2020;12(8).
[50] Castaneda P, et al. Biofilm antimicrobial susceptibility increases with antimicrobial exposure time. Clin Orthop Relat Res 2016;474(7):1659–64.
[51] Heydorn A, Ersbøll BK, Vorregaard M. Comstat 2. 2015 May 31. p. 2023. Available from: http://www.comstat.dk/.
[52] Heydorn A, et al. Quantification of biofilm structures by the novel computer program comstat. Microbiology 2000;146(10):2395–407.
[53] Sternberg C, et al. Comstat 2.1 manual. 1. 1 ed. Technical University of Denmark; 2015.
[54] Vorregaard M. Comstat2 - a modern 3D image analysis environment for biofilms. In: Informatics mathematical modelling. Denmark: Technical University of Denmark: Kongens Lyngby; 2008.